

Investigation of efficiency droop for InGaN-based UV light-emitting diodes with InAlGaN barrier

Po-Min Tu, Chun-Yen Chang, Shih-Cheng Huang, Ching-Hsueh Chiu, Jet-Rung Chang, Wei-Ting Chang, Dong-Sing Wu, Hsiao-Wen Zan, Chien-Chung Lin, Hao-Chung Kuo, and Chih-Peng Hsu

Citation: *Applied Physics Letters* **98**, 211107 (2011); doi: 10.1063/1.3591967

View online: <http://dx.doi.org/10.1063/1.3591967>

View Table of Contents: <http://scitation.aip.org/content/aip/journal/apl/98/21?ver=pdfcov>

Published by the [AIP Publishing](#)

Articles you may be interested in

Inserting a p-InGaN layer before the p-AlGaN electron blocking layer suppresses efficiency droop in InGaN-based light-emitting diodes

Appl. Phys. Lett. **101**, 081120 (2012); 10.1063/1.4747802

Effect of temperature and strain on the optical polarization of (In)(Al)GaN ultraviolet light emitting diodes

Appl. Phys. Lett. **99**, 261105 (2011); 10.1063/1.3672209

Optical polarization characteristics of ultraviolet (In)(Al)GaN multiple quantum well light emitting diodes

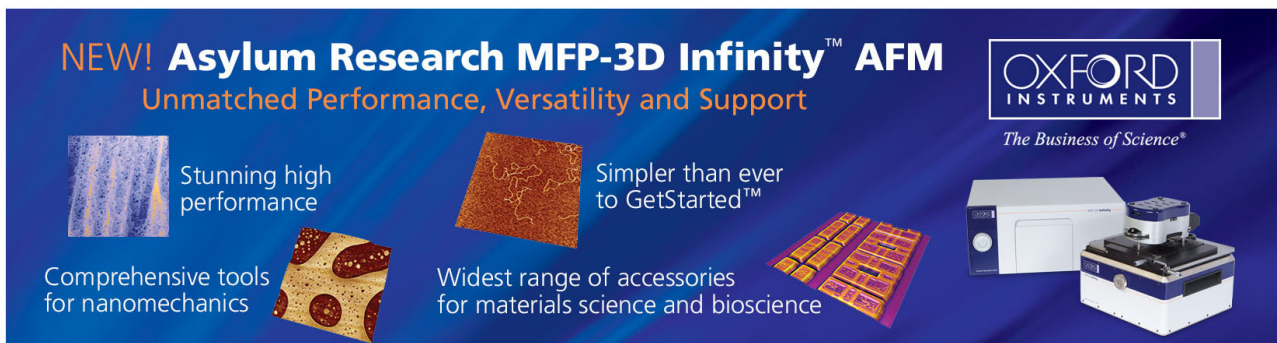
Appl. Phys. Lett. **97**, 171105 (2010); 10.1063/1.3506585

Influence of residual oxygen impurity in quaternary InAlGaN multiple-quantum-well active layers on emission efficiency of ultraviolet light-emitting diodes on GaN substrates

J. Appl. Phys. **99**, 114509 (2006); 10.1063/1.2200749

Quaternary InAlGaN-based high-efficiency ultraviolet light-emitting diodes

J. Appl. Phys. **97**, 091101 (2005); 10.1063/1.1899760



NEW! Asylum Research MFP-3D Infinity™ AFM
Unmatched Performance, Versatility and Support

OXFORD INSTRUMENTS
The Business of Science®

Stunning high performance
Simpler than ever to GetStarted™

Comprehensive tools for nanomechanics
Widest range of accessories for materials science and bioscience

Investigation of efficiency droop for InGaN-based UV light-emitting diodes with InAlGaN barrier

Po-Min Tu,¹ Chun-Yen Chang,^{2,a)} Shih-Cheng Huang,^{3,4} Ching-Hsueh Chiu,¹ Jet-Rung Chang,² Wei-Ting Chang,⁵ Dong-Sing Wu,³ Hsiao-Wen Zan,¹ Chien-Chung Lin,⁶ Hao-Chung Kuo,¹ and Chih-Peng Hsu⁴

¹Department of Photonics and Institute of Electro-Optical Engineering, National Chiao-Tung University, Hsinchu 300, Taiwan

²Institute of Electronics, National Chiao-Tung University, Hsinchu 300, Taiwan

³Department of Materials Science and Engineering, National Chung Hsing University, Taichung 402, Taiwan

⁴Advanced Optoelectronic Technology Inc., Hsinchu 303, Taiwan

⁵Department of Electro-Physics, National Chiao-Tung University, Hsinchu 300, Taiwan

⁶Institute of Photonic System, College of Photonics, National Chiao-Tung University, Tainan 711, Taiwan

(Received 21 February 2011; accepted 26 April 2011; published online 23 May 2011)

The efficiency droop in InGaN-based UV light emitting device (LED) with AlGa_{0.98}N and InAlGa_{0.98}N barrier is investigated. Electroluminescence results indicate that the light performance of quaternary LEDs can be enhanced by 25% and 55% at 350 mA and 1000 mA, respectively. Furthermore, simulations show that quaternary LEDs exhibit 62% higher radiative recombination rate and low efficiency degradation of 13% at a high injection current. We attribute this improvement to increasing of carrier concentration and uniform redistribution of carriers. © 2011 American Institute of Physics. [doi:10.1063/1.3591967]

GaN-based ultraviolet light emitting devices (LEDs) have attracted great attention in last few years due to its potential applications in photocatalytic deodorizing such as air conditioner,¹ and there have been interests in solid-state lighting by using near-UV LEDs light for the phosphor-converting source.^{2,3} However, external quantum efficiency (EQE) decreases drastically below the wavelength of 400 nm.⁴ It is well known that in low indium content InGaN quantum wells (QWs), AlGa_{0.98}N barrier is necessary for carrier confinement. But the two materials of AlGa_{0.98}N and InGaN are very different in growth temperature, which affects strongly on the quality of material and device performances. To improve the quantum efficiency of the InGaN-based LEDs, previous reports used InAlGa_{0.98}N in the quantum barrier instead of AlGa_{0.98}N or GaN for polarization, strain, material quality, and interfacial abruptness issues.^{5–8} However, by introducing of indium in AlGa_{0.98}N without increase aluminum content will cause the enhancement of the quantum confined Stark effect and other band gap issues. In this letter, the InAlGa_{0.98}N barrier was not for lattice or band gap matched in InGaN QW but matched in optimized AlGa_{0.98}N barrier, for a fair investigation on the light output and efficiency current droop characteristics.

All samples used in this letter were grown on 2" c-plane sapphire substrates using an atmospheric-pressure metal organic chemical vapor deposition (SR4000) system. For the growth of GaN-based LEDs, trimethyl gallium (TMGa), trimethyl indium (TMIn), trimethyl aluminum (TMAI), and ammonia (NH₃) were used as the source precursors for Ga, In, Al, and N, respectively. Silane (SiH₄) and bis-cyclopentadienyl magnesium (Cp₂Mg) were used as n-type and p-type dopants. The conventional structure is as follows. A 500 °C LT 30-nm-thick GaN nucleation layer was deposited, followed by a 1-μm-thick undoped GaN layer and a

2.5-μm-thick n-type Al_{0.02}Ga_{0.98}N layer grown at 1150 °C. A ten-period InGaN/AlGa_{0.98}N multi-QW (MQW) active region was grown at 830 °C. Subsequently, a 15-nm-thick Mg-doped Al_{0.3}Ga_{0.7}N and a 10-nm-thick Mg-doped Al_{0.1}Ga_{0.9}N electron-blocking layers (EBLs) were grown at 1050 °C, followed by a 60-nm-thick Mg-doped GaN contact layer grown at 1030 °C. The quaternary structure of InGaN/InAlGa_{0.98}N MQW was almost identical to that of the InGaN/AlGa_{0.98}N MQW LED, the only difference was that we used InAlGa_{0.98}N instead of AlGa_{0.98}N as the barrier layers in the active region. Here, the MQW active region consisted of ten periods of 2.6-nm-thick undoped In_{0.025}Ga_{0.975}N well layers and 11.7-nm-thick Si-doped In_{0.0085}Al_{0.1112}Ga_{0.8803}N or Al_{0.08}Ga_{0.92}N barrier layers growth on n-Al_{0.02}Ga_{0.98}N/ud-GaN/sapphire. During the growth of barriers, we kept the flow rates of TMGa, NH₃, and SiH₄ at 12.24 μmol/min, 0.67 mol/min, and 0.196 nmol/min. For the growth of InAlGa_{0.98}N, we added the flow rate of TMIn for 0.79 μmol/min and increased the flow rate of TMAI from 1.94 μmol/min to 2.13 μmol/min, compared to AlGa_{0.98}N barrier. To probe the detailed properties of epitaxial layers, a 50 nm InAlGa_{0.98}N and AlGa_{0.98}N single heteroepitaxial layers were also deposited on n-AlGa_{0.98}N/ud-GaN/sapphire substrate. The mole fractions of Al and In in MQWs were identified by double crystal x-ray diffraction (DCXRD, Bede D1, U.K.) using Cu Kα1 (λ=1.54056 Å) as source. These samples were also characterized by photoluminescence (PL), atomic force microscopy (AFM) and transmission electron microscopy (TEM) to reveal the optical property, surface morphology, and MQWs structure, respectively. Finally, the UV LED wafers were processed into mesa-type chips (size: 1 mm × 1 mm) and packaged on epoxy-free metal cans (TO-66, thermal resistance (R_θ) ~ 2 K/W). The output power of the UV LED was measured using an integrated sphere detector and tested at room temperature with currents up to 1 A. Testing is done in pulsed mode with 100 μs pulses and a 1% duty cycle to prevent self-heating because the thermal time

^{a)}Electronic mail: cyc@mail.nctu.edu.tw.

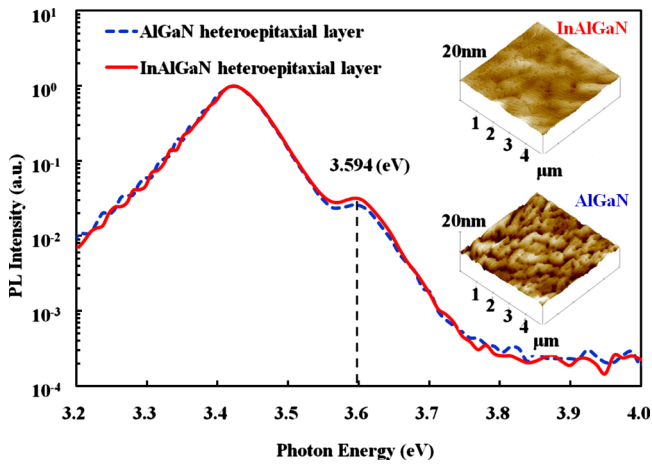


FIG. 1. (Color online) Room-temperature PL spectra of AlGaN and InAlGaN single heteroepitaxial layers. Inset in Fig. 1 shows surface morphology AFM over $5 \times 5 \mu\text{m}^2$ of AlGaN (RMS: 0.813 nm) and InAlGaN (RMS: 0.595 nm) layer with thickness about 50 nm.

constant of the LEDs is in the millisecond range.⁹ In this letter, the optical and electrical properties of InGaN/InAlGaN and conventional InGaN/AlGaN MQW LEDs are numerically calculated using the APSYS simulation software.¹⁰

PL spectra of AlGaN and InAlGaN single heteroepitaxial layers grown on n-AlGaN/ud-GaN/sapphire substrate were obtained at a room temperature to investigate the band edge emission. Figure 1 shows that the PL emission energy of these two samples are very close (about 3.594 eV) and the peak intensity of InAlGaN is slightly higher than AlGaN. The strong PL emission is attributed to the better crystal quality. Inset in Fig. 1 shows the surface morphology of the two AlGaN and InAlGaN single heteroepitaxial layers with the same thickness about 50 nm. The root-mean-square (RMS) roughness measured by AFM is about 0.813 nm and 0.595 nm, respectively. The relatively high roughness of AlGaN single heteroepitaxial layer can mainly be attributed to the low deposition temperature of 830 °C necessary for the adjacent InGaN well.

Figure 2(a) shows the XRD (ω - 2θ) curves in the (002) reflections of InGaN/AlGaN and InGaN/InAlGaN MQWs. The results show that the locations of multiple satellite peaks of InGaN/AlGaN and InGaN/InAlGaN MQWs are very close. This indicates that the thickness of barrier layer in these two samples is matched and it is quite consistent with the measured values of 11.7 nm from HRTEM images as shown in Figs. 2(b) and 2(c). In addition to experimentally estimate the indium and aluminum composition in the MQWs, we simulate the XRD (ω - 2θ) curve by using dynamical diffraction theory. The In composition in the QWs was determined to be about 2.5%, where the thickness of the well was about 2.6 nm. The compositions of ternary and quaternary barriers were $\text{Al}_{0.08}\text{Ga}_{0.92}\text{N}$ and $\text{In}_{0.0085}\text{Al}_{0.1112}\text{Ga}_{0.8803}\text{N}$, respectively. Besides, the growth rates of well and barrier were estimated about 0.329 Å/s and 0.308 Å/s, respectively.

The optical properties of UV LED with ternary and quaternary barrier are shown in Fig. 3. Figure 3(a) shows the light output power-current-voltage (L-I-V) characteristics for the AlGaN and InAlGaN barrier UV LEDs. The forward voltage was 3.89 V and 3.98 V for InGaN/AlGaN and InGaN/InAlGaN MQWs UV LED at a forward current of

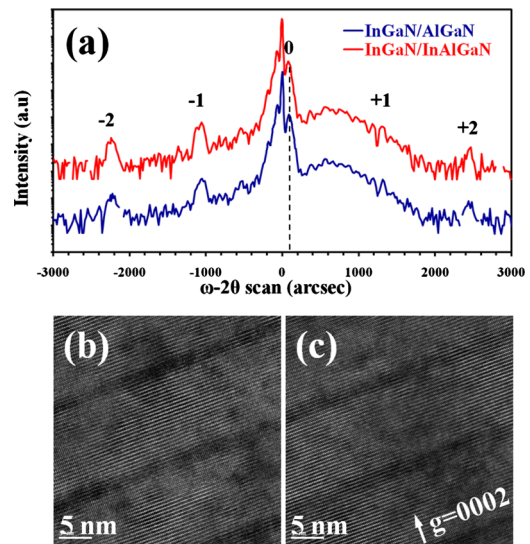


FIG. 2. (Color online) (a) XRD (ω - 2θ) curves in the (002) reflections of InGaN/AlGaN and InGaN/InAlGaN MQW. Cross-sectional TEM images of (b) InGaN/AlGaN and (c) InGaN/InAlGaN MQW. The diffraction condition is $g=0002$.

350 mA, respectively. A little high forward voltage of InAlGaN barrier LED can be attributed to the higher Al content compare to the AlGaN barrier, thus increase the series resistance in the device. The light output power of InGaN-based UV LED with the InAlGaN barrier is higher by 25% and 55% than the AlGaN barrier at 350 mA and 1000 mA, respectively. Figure 3(b) shows the normalized efficiency curves of experimental (open circles) and simulated (solid lines) as a function of forward current for the two samples. For the InGaN/AlGaN UV LEDs, when the injection current exceeds 1000 mA, the efficiency is reduced to 66% of its maximum value. In contrast, InGaN/InAlGaN UV LEDs exhibit only 13% efficiency droop when we increase the injection current to 1000 mA. The reduction in efficiency

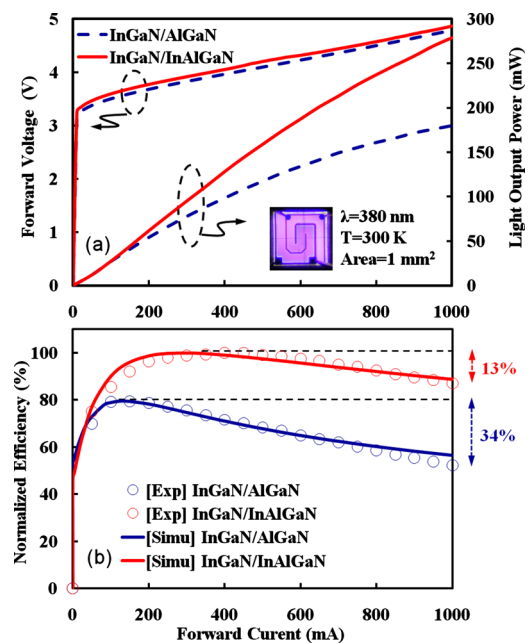


FIG. 3. (Color online) (a) L-I-V curves of the LEDs with AlGaN (dash) and InAlGaN (solid) barrier. (b) Normalized efficiency curves of experimental (open circles) and simulated (solid lines). Inset in Fig. 3(a) shows the mesa-type UV chip.

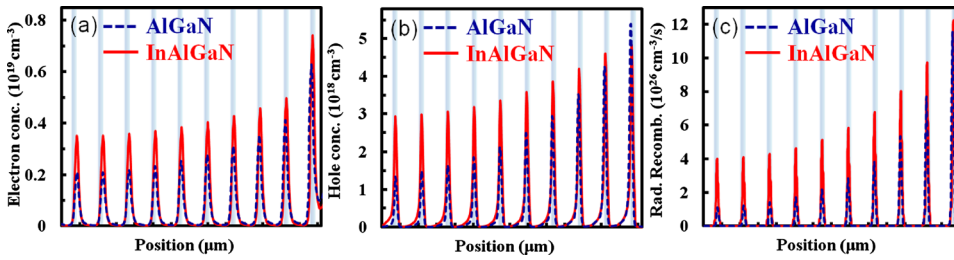


FIG. 4. (Color online) Distribution of (a) electron, (b) hole concentrations, and (c) radiative recombination rates of the LEDs with AlGaIn and InAlGaIn barrier under a high forward current density of 100 A/cm².

droop is quite clear and the current at maximum efficiency shifts from 150 to 400 mA. Besides, the wavelength is nearly constant about 380 nm over the entire current range. The absence of temperature-induced redshift suggests that self-heating is substantially suppressed by using metal type packaging and pulsed mode operating.¹¹ In order to investigate the physical origin of efficiency droop in these UV LEDs, we performed a simulation of the above structures by using the APSYS simulation software. Commonly accepted Shockley–Read–Hall recombination lifetime (about ~ 6 ns) and Auger recombination coefficient (about $\sim 10^{-30}$ cm⁶ s⁻¹) are used in the simulations. Other material parameters of the semiconductors used in the simulation can be found in Ref. 12. In addition, we can reduce the effect of spontaneous and piezoelectric polarizations because of lattice match condition in barrier between AlGaIn and InAlGaIn. The total polarization fields in different combination of materials can be obtained through the calculation, and the results of In_{0.025}Ga_{0.975}N, Al_{0.08}Ga_{0.92}N, and In_{0.0085}Al_{0.112}Ga_{0.8803}N are the -0.0305 (C m⁻²), -0.0391 (C m⁻²), and -0.0398 (C m⁻²), respectively.¹³ Besides, a different band-offset ratio from 6:4 to 7:3 is used in this simulation for introducing of indium in AlGaIn. We can know that under the same energy band of barrier, the band-offset ratio from 6:4 to 7:3 will lead higher conduction-band and lower valence-band between well and barrier. This is useful for electron confinement and hole distribution in low indium content InGaIn-based UV LEDs. However, another difficult problem is the inclusion of degenerate valence bands in minority carrier hole mobility. Hence, to investigate the efficiency droop in these two samples, we assume that InGaIn-based UV LED with InAlGaIn barrier has relatively high carrier mobility. The values of mobility for electron and hole are assumed in the simulation, $\mu_{n-\text{InGaIn/AlGaIn}}=354$ cm²/V s, $\mu_{n-\text{InGaIn/InAlGaIn}}=642$ cm²/V s, $\mu_{p-\text{InGaIn/AlGaIn}}=2$ cm²/V s, and $\mu_{p-\text{InGaIn/InAlGaIn}}=5$ cm²/V s, respectively. Finally, the results of the EQE droop simulation of both different structures are in good agreement with the experimental data as shown in Fig. 3(b). Finally, we have to check the actual carrier distribution in our simulation. Figure 4 shows the calculated carrier distribution in these UV LEDs structure under a high forward current density of 100 A/cm² (1000 mA) by APSYS. When we apply the corresponding band-offset ratio and the carrier mobility in InGaIn/InAlGaIn MQWs, the electron and hole concentration increases in the QW by about 26% and 35%, respectively, and the distribution of carrier becomes more uniform than InGaIn/AlGaIn case. Under high current density, the carrier distribution of both electrons and holes determines how efficient the photon-emission process will be. As shown in Fig. 4, the peak-to-peak carrier ratio of InAlGaIn barrier sample is reduced due to better carrier transportation and this is also more obvious in the hole distribution. The direct consequence is the increasing radiative

recombination rate and thus the light output is expected to rise. On the other hand, in the traditional AlGaIn barrier samples, the holes are locally concentrated in the first QW, which causes the unbalanced distribution between different types of carriers and thus leads to reduction in radiative recombination rate. Comparing electrons and holes, holes suffer more as a result of this nonuniformity due to their large effective mass and low mobility. Thus, our InAlGaIn design can reduce the carrier leakage and increase electron-hole pair radiative recombination simultaneously, especially for the distribution of holes.

In summary, we fabricated and compared the performance of LEDs of InGaIn-based UV MQWs active region with ternary AlGaIn and quaternary InAlGaIn barrier layers. XRD and TEM measurements show the two barriers are consistent with the lattice and smooth morphology of quaternary InAlGaIn layer can be observed in AFM. The electroluminescence results indicate that the light performance of the InGaIn-based UV LEDs can be enhanced effectively when the conventional low temperature AlGaIn barrier layers are replaced by the InAlGaIn barrier layers. Furthermore, simulation results show that InGaIn-based UV LEDs with quaternary InAlGaIn barrier exhibit 62% higher radiative recombination rate and low efficiency droop of 13% at a high injection current. We attribute this improvement to increasing in carrier concentration and uniform redistribution of carriers.

The authors are grateful to the National Science Council of the Republic of China, Taiwan, for financially supporting this research under Contract Nos. NSC 98-2221-E-009-003 and NSC 99-ET-E-009-001-ET.

¹A. Sandhu, *Nat. Photonics* **1**, 38 (2007).

²Y. S. Tang, S. F. Hu, C. C. Lin, N. C. Bagkar, and R. S. Liu, *Appl. Phys. Lett.* **90**, 151108 (2007).

³Y. C. Chiu, W. R. Liu, C. K. Chang, C. C. Liao, Y. T. Yeh, S. M. Jang, and T. M. Chen, *J. Mater. Chem.* **20**, 1755 (2010).

⁴H. Hirayama, *J. Appl. Phys.* **97**, 091101 (2005).

⁵A. Knauer, H. Wenzel, T. Kolbe, S. Einfeldt, M. Weyers, M. Kneissl, and G. Tränkle, *Appl. Phys. Lett.* **92**, 191912 (2008).

⁶M. F. Schubert, J. Xu, J. K. Kim, E. F. Schubert, M. H. Kim, S. Yoon, S. M. Lee, C. Sone, T. Sakong, and Y. Park, *Appl. Phys. Lett.* **93**, 041102 (2008).

⁷J. J. Wu, G. Y. Zhang, X. L. Liu, Q. S. Zhu, Z. G. Wang, Q. J. Jia, and L. P. Guo, *Nanotechnology* **18**, 015402 (2007).

⁸S. H. Baek, J. O. Kim, M. K. Kwon, I. K. Park, S. I. Na, J. Y. Kim, B. J. Kim, and S. J. Park, *IEEE Photon. Technol. Lett.* **18**, 1276 (2006).

⁹Q. Shan, Q. Dai, S. Chhajed, J. Cho, and E. F. Schubert, *J. Appl. Phys.* **108**, 084504 (2010).

¹⁰APSYS by Crosslight Software Inc., Burnaby, Canada: <http://www.crosslight.com>.

¹¹Y. Yang, X. A. Cao, and C. Yan, *IEEE Trans. Electron Devices* **55**, 1771 (2008).

¹²F. Bernardini, in *Nitride Semiconductor Devices: Principles and Simulation*, edited by J. Piprek (Wiley, New York, 2007), pp. 49–67.

¹³M. H. Kim, M. F. Schubert, Q. Dai, J. K. Kim, E. F. Schubert, J. Piprek, and Y. Park, *Appl. Phys. Lett.* **91**, 183507 (2007).